Journal of Neuroendocrinology

Journal of Neuroendocrinology, 2015, **27**, 835–849

ORIGINAL ARTICLE

Localisation of 11β-Hydroxysteroid Dehydrogenase Type 2 in Mineralocorticoid Receptor Expressing Magnocellular Neurosecretory Neurones of the Rat Supraoptic and Paraventricular Nuclei

M. Haque, R. Wilson, K. Sharma, N. J. Mills and R. Teruyama

Department of Biological Sciences, Louisiana State University, Baton Rouge, LA, USA.

Journal of Neuroendocrinology

Correspondence to: Ryoichi Teruyama, Louisiana State University, 202 Life Sciences Building, Baton Rouge, LA 70803, USA (e-mail: rteruyama@lsu.edu).

An accumulating body of evidence suggests that the activity of the mineralocorticoid, aldosterone, in the brain via the mineralocorticoid receptor (MR) plays an important role in the regulation of blood pressure. MR was recently found in vasopressin and oxytocin synthesising magnocellular neurosecretory cells (MNCs) in both the paraventricular (PVN) and supraoptic (SON) nuclei in the hypothalamus. Considering the physiological effects of these hormones, MR in these neurones may be an important site mediating the action of aldosterone in blood pressure regulation within the brain. However, aldosterone activation of MR in the hypothalamus remains controversial as a result of the high binding affinity of glucocorticoids to MR at substantially higher concentrations compared to aldosterone. In aldosterone-sensitive epithelia, the enzyme 11β-hydroxysteroid dehydrogenase type 2 (11β-HSD2) prevents glucocorticoids from binding to MR by converting glucocorticoids into inactive metabolites. The present study aimed to determine whether 11β-HSD2, which increases aldosterone selectivity, is expressed in MNCs. Specific 11β-HSD2 immunoreactivity was found in the cytoplasm of the MNCs in both the SON and PVN. In addition, double-fluorescence confocal microscopy demonstrated that MR-immunoreactivity and 11β-HSD2-*in situ* hybridised products are colocalised in MNCs. Lastly, single-cell reverse transcriptase-polymerase chain reaction detected MR and 11β-HSD2 mRNAs from cDNA libraries derived from single identified MNCs. These findings strongly suggest that MNCs in the SON and PVN are aldosterone-sensitive neurones.

Key words: oxytocin, vasopressin

doi: 10.1111/jne.12325

Magnocellular neurosecretory cells (MNCs) in the supraoptic (SON) and paraventricular (PVN) nuclei synthesise and release the neurohypophysial hormones, vasopressin (VP) and oxytocin (OT), from terminals in the posterior lobe of the pituitary. These two hormones are released into the general circulation in response to decreases in blood volume, pressure or extracellular fluid tonicity. VP plays an important role in the elevation of blood pressure by exerting vasoconstricting and antidiuretic actions in the kidney (1,2). OT acts as a natriuretic factor promoting sodium excretion by the kidney (3,4), in addition to the well-known effects of OT in female reproduction; OT promotes the contraction of both smooth muscle in the uterus during labour and in myoepithelial cells in the mammary gland during milk ejection (5). In addition to VP and OT synthesising MNCs, parvocellular neurones are located in both the dorsal cap and ventrolateral subdivisions of the PVN. Some parvocellular neurones are presympathetic, affecting renal sympathetic outflow supporting the maintenance of the fluid/electrolyte balance (6,7). Because the activity of parvocellular presympathetic neurones is, at least partly, regulated by the somatodendritic release of VP from MNCs within the PVN (8), VP coordinates neurohumoral homeostatic responses via cross-talk between the MNCs and the autonomic parvocellular cells in the PVN. MNCs therefore precisely coordinate neuroendocrine and autonomic responses to maintain optimal blood pressure within a constantly changing physiological condition.

We recently demonstrated that the nonvoltage-dependent, amiloride-sensitive epithelial Na^+ channels (ENaCs) are present in the MNCs and mediate a Na^+ leak current that modulates the membrane potential of MNCs (9). Because the release of OT and VP hormones from the neurohypophysis depends largely on the frequency and pattern of action potentials in their synthesising

neurones (2,10), the presence of ENaC in MNCs implies that activation of ENaC comprises one way of modulating hormone secretion according to physiological demands. Expression of ENaC in epithelia is largely regulated by aldosterone through the mineralocorticoid receptor (MR) (11–15). The presence of MR in MNCs (9,16–20) therefore indicates that ENaC expression in MNCs may also be promoted by aldosterone. However, not only is there no information regarding the physiological functions of MR in MNCs, but also aldosterone activation of MR in the hypothalamus is also controversial. Because MR binds with high affinity to aldosterone as well as to corticosteroids (21–24), and because the concentration of corticosterone in the brain is substantially higher than that of aldosterone, MRs in the brain are considered to be largely occupied by corticosterone (25). Aldosterone-sensitive epithelial tissues express the enzyme, 11β-hydroxysteroid dehydrogenase type 2 (11β-HSD2), which converts corticosterone into an inactive metabolite to increase aldosterone selectivity to MR (26–28). Thus, the co-localisation of MR and 11β-HSD2 in the same cells indicates that the cells are sensitive to aldosterone (29–31).

Although several studies using the reverse transcriptase-polymerase chain reaction (RT-PCR) consistently detected 11β-HSD2 mRNA in both the hypothalamus (32–36) and in tissue micropunches from the PVN (35), these studies provided no cellular localisation of 11β-HSD2 in the hypothalamus. *In situ* hybridisations of 11β-HSD2 in rat brain were reported previously, although no specific labelling in the SON or PVN was reported (37–39). However, these *in situ* hybridisation studies were not intended to specifically detect 11β-HSD2 mRNA in MNCs or in the hypothalamus, and the autoradiographical method was probably not sufficiently sensitive to detect relatively limited mRNA at the cellular level. More recently, immunocytochemical localisations of 11β-HSD2 in the brain were reported, although no immunoreactivity to 11β-HSD2 in the PVN was found (40,41). The antibody used in these previous studies, however, shows nonspecific binding in the cellular nuclei, and thus a more diluted concentration was needed. Although this approach was adequate for detecting cells that express relatively abundant amounts of 11β-HSD2, such as cells in the nucleus of the solitary tract known to regulate sodium appetite in response to aldosterone (40), the study might have overlooked the relatively scarce amount of 11β-HSD2 in the MNCs. The present study therefore specifically aimed to re-evaluate the presence of 11β-HSD2 in MR-expressing MNCs in both the SON and PVN using experimental techniques of immunocytochemistry, *in situ* hybridisation and single-cell RT-PCR.

Materials and methods

Animals

Male Wistar and Wistar–Kyoto (WKY) rats were examined (320–380 g body weight; Harlan Laboratories, Indianapolis, IN, USA). The rats with access to food and water available *ad lib.* were housed in a room under a 12 : 12 h light/dark cycle. All protocols were approved by the Institutional Animal Care and Use Committee at Louisiana State University.

Immunocytochemistry

Animals were deeply anaesthetised with sodium pentobarbital (50 mg/kg, i.p.) and transcardially perfused with 0.01 M sodium phosphate-buffered saline (PBS) (pH 7.2) followed by 4% paraformaldehyde in 0.1 M sodium phosphate buffer (PB, pH 7.2). The heads were postfixed in the same fixative for 1–3 days. The brains were extracted and infiltrated with 20% sucrose in 0.1 M PB until they sank to the bottom or for overnight. The coronal sections at 40 μm were obtained by a sliding microtome (SM2010R; Leica, Mannheim, Germany).

Free-floating brain sections were incubated with a monoclonal anti-MR antibody or polyclonal anti-11β-HSD2 antibody diluted in PBS containing 0.5% Triton X-100 for 48–72 h at 4 °C. Four different anti-MR monoclonal antibodies (rMR365 4D6, rMR1-18 1D5, MRN2 2B7 and MRN3 3F 10), developed by C. E. Gomez-Sanchez, were obtained from the Developmental Studies Hybridoma Bank developed under the auspices of the NICHD and maintained by Department of Biology, The University of Iowa (Iowa City, IA, USA). All of these antibodies in our pilot study displayed essentially identical distribution of immunoreactivity in the hypothalamic region. MRN3 3F10 was selected for the present study because it showed the most robust immunoreactivity in the hypothalamus. The production and characterisation of these MR antibodies have been described in great detail previously (42). A range of different antibody dilutions was tested (1 : 100 to 1 : 10 000) for anti-MR and a dilution of 1 : 500 produced optimal signal-to-noise. The polyclonal anti-11β-HSD2 antibody was raised against a synthetic peptide corresponding to amino acids of 129–400 (polyhistidine N-terminal) from rat 11β-HSD2 (AB1296; Chemicon, Temecula, CA, USA). Characteristics of the 11β-HSD2 antibody in immunocytochemistry was initially tested at dilutions between 1 : 5000 and 1 : 80 000 in nine animals. Consistent with the report of Geerling *et al.* (43), this antibody labelled all neuronal nuclei at dilution under 1 : 25 000. Although we agree with the interpretation of the ubiquitous nuclear labelling at higher antibody concentrations being nonspecific cross-reactivity, careful observation of sections treated with the antibody at dilutions below 1 : 10 000 revealed that 11β-HSD2 immunoreactivity was also observed in the cytoplasm of MNCs in the SON and the PVN. A dilution of 1 : 10 000 for anti-11β-HSD2 antibody produce optimal signal-to-noise staining of the cytoplasm of MNCs in the SON and PVN. Omission of the primary antibody was used as a negative control and produced no detectable immunoreactivity. In addition, immunocytochemistry of anti-11β-HSD2 antibody was tested on the kidney sections where the presence of 11β-HSD2 is known (44).

For light microscopy, the brain sections were subsequently incubated with appropriate biotinylated secondary antibodies (dilution 1 : 200; Vector, Burlingame, CA, USA) followed by the standard ABC-diaminobenzidine (DAB) procedure per the protocol provided by Vector. The brain sections were mounted on gelatin-coated slides, dehydrated, cleared and cover slipped with Permount. Light microscopic images were acquired digitally with a microscope (Nikon Eclipse 80i; Nikon, Tokyo, Japan) equipped with a digital camera (Nikon DS-QiMc). Digital images were minimally altered in IMAGEJ (NIH, Bethesda, MD, USA) with changes in dynamic range.

For double-immuno labeling of MR with VP or OT, specific anti-VP-neurophysin (VP-NP) and OT-NP polyclonal antibodies raised in rabbits were used at a 1 : 20 000 dilution (provided by Alan Robinson, UCLA, CA). First, the brain sections were incubated with MRN3 3F10 as described above and labeled with DyLight 488-conjugated goat anti-mouse IgG (1 : 500; Jackson ImmunoResearch, West Grove, PA, USA). The MR-labeled brain sections were subsequently incubated with anti-VP-NP or anti-OT-NP antibody for overnight and labeled with DyLight 649-conjugated goat anti-rabbit IgG (1 : 500; Jackson ImmunoResearch). The brain sections were examined and confocal images were acquired at 1024 × 1024 format (Leica TCS SP2 spectral confocal microscope, Mannheim, Germany). The optical sections were 1 μm thick and viewed in stacks of three sections using ImageJ software (NIH).

Optical density (OD) measurements of immunocytochemistry

Brain sections obtained from six brains from each of the Wistar and WKY rats were treated for MR-immunocytochemistry concurrently under the same conditions. Digital photomicrographs of both sides of the SON (n = 6) were acquired every 200 μm from DAB-stained brain sections that contained the nucleus. Each image was digitised with 12-bit intensity levels using a microscope (Nikon Eclipse 80i) equipped with a digital camera (Nikon DS-QiMc). All images were taken at the same exposure (time and length) and light intensity. Average OD value of densitometric measurements of the entire SON and the magnocellular division of the PVN were obtained from the photomicrographs using IMAGEJ (NIH). To normalise OD values, areas outside the SON and PVN OD value were subtracted from the averaged SON and PVN OD values, respectively, in each image.

Semi-quantitative real-time RT-PCR

The rats were deeply anaesthetised with sodium pentobarbital (50 mg/kg, i.p.) and perfused through the heart with ice-cold modified an artificial cerebral spinal fluid (aCSF) solution in which NaCl was replaced by equiosmolar sucrose containing (in mM): 210 sucrose, 3 KCl, 2.0 $CaCl_2$, 1.3 $MgCl_2$, 1.24 NaH_2PO_4, 25 $NaHCO_3$, 0.2 ascorbic acid and 10 D-glucose (pH 7.4). The brains were removed and sliced in the coronal plane in ice-cold aCSF at a thickness of 500 μm using a vibrating microtome (VT1200; Leica). SON tissues were collected from six age-matched male rats for each Wistar and WKY strain using a punch-tool (inner diameter 1.0 mm) that allowed obtaining tissue only from the SON.

The micropunched samples were placed in *RNAlater* (Qiagen, Valencia, CA, USA) and stored at −20 °C until sampling from all the animals were completed. Total RNA was isolated from the samples using TRI reagent (Sigma-Aldrich, St Louis, MO, USA) after lysis in a tissue lyser (Qiagen). The concentration and quality of the isolated RNA was determined using a NanoDrop spectrophotometer (Thermo-Fisher Scientific, Waltham, MA, USA). After *DNase*I treatment, equal amount of RNA was reverse transcribed to cDNA using oligo dT and M-MLV reverse transcriptase (Sigma-Aldrich). Real-time PCR was performed using SYBR Select Master Mix (ABI Applied Biosystems, Grand Island, NY, USA) with ABI ViiA-7 sequence detection system (Applied Biosystems). Primers were specifically designed from exon spanning region to exclude the potential amplification of any genomic DNA and to amplify the cDNA of interest. The Primer sets used for MR were (forward: 5′-CTCCCTAACATGTCCTAGAAAAGC-3′ and reverse: 5′-AGAACGCTCCAAGGTCT GAG-3′; accession # NM 013131.1) and cyclophilin B (forward: 5′-CTTGGTG TTCTCCACCTTCC-3′ and reverse: 5′-ACGTGGTTTTCGGCAAAGT-3′; accession #NM 022536.1). The RT-PCR reaction for each sample was performed in triplicate and the average cycle threshold (Ct) was obtained. To normalise the expression of *MR*, the differences in Ct (ΔCt) were obtained by subtracting the Ct of MR from Ct of cyclophilin B. The relative differences in the expression of MR between Wistar and WKY rats were obtained by subtracting mean ΔCt and expressed as ΔΔCt.

In situ hybridisation

Tissue preparation. The brain sections were prepared as described above with respect to immunocytochemistry.

Preparation of the probe. cDNA was prepared using total RNA extracted from rat SON punches. From this cDNA, 11β-HSD2 PCR products were made using a probe primer set (forward: GAT TTA GGT GAC ACT ATA GAA ggacgtattgtgaccgttgg, reverse: CTAA TAC GAC TCA CTA TAG GGA C gctggatgatgctgaccttg), which contains promoters for both Sp6 and T7 RNA polymerase. The amplified DNA was purified using a PCR clean up Column (Sigma-Aldrich). A nonradioactive digoxigenin (DIG) RNA labelling kit (Roche Diagnostics, Indianapolis, IN, USA) was used to synthesise sense and antisense DIG-labelled RNA probes for 11β-HSD2 using SP6 and T7 RNA polymerase (Roche Applied Science, Penzberg, Germany). This probe hybridises with 760–910 nucleotides of 11β-HSD2. The transcription reaction was performed in accordance with the manufacturer's protocol; briefly, 20 μl of the reaction mixture containing 2 μl of the transcription buffer, 2 μl of the labelling mixture, 2 μl of RNA polymerase and 1 μg of DNA were incubated for 2 h at 37 °C. Free nucleotides were separated on the PCR clean up column (Sigma-Aldrich). A DIG-labelled RNA probe was added to the hybridisation buffer at 100 ng/ml and denatured at 75 °C for 10 min.

Hybridisation. Free-floating brain sections were pre-incubated in hybridisation buffer consisting of 200 mM NaCl, 10 mM Tris HCl (pH 7.5), 10 mM phosphate buffer, 5 mM ethylenediaminetetraacetic acid, 50% formamide, 10% dextran sulphate and 1× Dehardt's solution at 55 °C for 1 h on a rocker incubator (Boekel Scientific, Feasterville, PA, USA). The buffer was then replaced with the denatured probe and incubated at the same temperature overnight. Brain sections were then washed for 30 min with the washing buffer (1× saline-sodium citrate buffer, 50% formamide, 0.1% Tween 20). The washing process was repeated three times to ensure that any residue components were removed. Subsequently, the sections were treated with the blocking reagent (Roche) in 1× maleic acid buffer (MAB: 100 mM maleic acid and 150 mM NaCl, pH 7.5) for 1 h and were then incubated at room temperature for 2 h in alkaline phosphatase conjugated anti-DIG antibody at 1 : 2000 dilution (Roche Applied Science). The brain sections were washed three times (10 min each) in 1× MAB-T (MAB containing 0.1% Tween 20). The hybrids were visualised in 5-bromo-4-chloro-3-indolyl phosphate (BCIP)- nitroblue tetrazolium (NBT)- polyvinyl alcohol (PVA) solution [10% PVA in 100 mM Tris HCl (pH 9) containing 0.2 mM BCIP, 0.2 mM NBT, and 5 mM $MgCl_2$] at 30 °C. Colour development was terminated by washing in water, and sections were mounted on gelatin coated microslides, dehydrated in ethanol gradient, clarified in xylene and cover slipped with permount. The brain sections were examined and images were acquired at 1280 × 1024 format with a light microscope (Nikon Eclipse 80i).

Control experiments. To check for the specificity of the hybridisation signals, sense versions of the probe were processed in parallel with the experimental specimens and found to lack any labelling for 11β-HSD2. The hybridisation was also tested on the kidney sections where the presence of 11β-HSD2 is known (44).

Double-labelling of 11β-HSD2 *in situ* hybridisation and MR immunocytochemistry

The sections that were hybridised with the DIG-labelled11β-HSD2 probe were incubated with sheep anti-digoxigenin antibody (0.5 μg/ml; Roche) for 2 h at room temperature. The sections were then incubated for 2 h with anti-sheep-antibody conjugated with DyLight 647 (dilution 1 : 400: Jackson Immuno Research, West Grove, PA, USA). Subsequently, the hybridised sections were incubated with MR antibody as described above for the immunocytochemistry and then labelled with anti-mouse antibody conjugated with DyLight 488 (dilution 1 : 400: Jackson Immuno Research). The sections were washed three times for 10 min between each step with appropriate buffers. Finally, sections were mounted in PVA with anti-fading agent 1,4-diazabicyclo[2.2.2]octane (DABCO) that consists of 4.8 g PVA, 12 g glycerol, 12 ml dH_2O, 24 ml 0.2 M Tris-HCl and 1.25 g DABCO. Brain slices were examined and confocal images (TCS SP2 spectral confocal microscope; Leica) were acquired at 1024 × 1024 format. The optical sections were 0.5 or 1 μm thick and viewed in stacks of 1–3 sections using IMAGEJ (NIH).

Single-cell RT-PCR

Single cell harvest for single-cell RT-PCR

Punched SON tissues were prepared as described above for the semi-quantitative real-time RT-PCR and were incubated in oxygenated aCSF (35 °C) containing Protease Type XIV (1.2 mg/ml; Sigma Chemicals, St Louis, MO, USA) for 20–30 min and washed in a solution consisting of (in mM): 140 sodium isethionate, 2 KCl, 4 $MgCl_2$, 23 glucose and 15 HEPES (pH 7.3) (adjusted with 1 M NaOH). The enzyme-treated tissue was triturated in sodium isethionate solution using three successively smaller fire-polished pipettes to release individual MNC cell bodies. The supernatant containing dissociated neurones was then transferred to a plastic Petri dish (Nunc, Rochester, NY, USA) on an inverted microscope stage and allowed to settle for approximately 5 min. Glass capillary tubes for pipettes (Corning 7052 capillary glass; Garner Glass, Claremont, CA, USA) were autoclaved to prevent RNase contamination. Electrodes were pulled on a Flaming/Brown micropipette puller (Model P-97; Sutter Instrument, Novato, CA, USA) and filled with RNase free water. Positive pressure was applied when the electrode approached a cell to minimise contamination (i.e. extracellular matrix, dead cells, RNase). Dissociated MNCs can be easily and reliably identified by their large cell size (> 16 μm in diameter). Negative pressure was applied to the electrode to draw the cell into the electrode. Following aspiration, the contents of the electrode were ejected into an ice-cold 0.5 ml PCR tube and stored at −80 °C.

First round multiplexed amplification

iTaq universal SYBR green one-step kit (Bio-Rad, Hercules, CA, USA) was used to make cDNA and amplification of the transcript in the same tube using gene specific primers. iTaq universal SYBR green mix, iScript reverse transcriptase and mixture of gene specific primers (forward and reverse primes for MR, 11β-HSD2, OT and VP) were added to the cell lysate, and thermo-cycling parameters were set in accordance with the manufacturer's instructions: 10 min at 50 °C (reverse transcription) and 1 min at 95 °C (polymerase activation and DNA denaturation) followed by 15 cycles of amplification (10 s at 95 °C and 1 min at 60 °C).

PCR

The amplified templates generated in the first round were subjected to conventional PCR using a programmable thermal cycler (Bio-Rad) and primers specifically designed to amplify the cDNA of interest (Table 1). The identification of each cDNA species is based on the predicted size of each PCR product on agarose gel. Negative controls for contamination from extraneous and genomic DNA from other sources were tested for each batch of neurones.

Table 1. Primer sequences used to detect gene expressions of interest.

Gene		Primer sequence	Amplicon size (bp)
11βHSD2	F	5′-TCAGCCGTGTTCTGGAAATTA-3′	123
	R	5′-GGAAAGTTACCACTGGAGACAG-3′	
MR	F	5′-GGTATCCCGTCCTAGAGTACAT-3′	196
	R	5′-AGATAGTTGTGTTGCCCTTCC-3′	
OT	F	5′-GCCTGCTTGGCCTACTG-3′	109
	R	5′-CCGCAGGGAAGACACTTG-3′	
VP	F	5′-CACCTATGCTCGCCATGAT-3′	299
	R	5′-GCTTCCGCAAGGCTTCT-3′	

Results

Localisation of MR in the hypothalamus

Within the hypothalamic region, marked MR-immunoreactive neurones were observed only in the SON and PVN (Fig. 1A,B). Strong MR immunoreactivity was largely confined to the cell body in a majority of MNCs in the SON (Fig. 1C). Overall immunolabelling in the PVN was weaker compared to that in the SON; however, prominent immunoreactive neurones were observed in the magnocellular region of the PVN. Empirical evidence obtained in our laboratory showed that WKY rats (Fig. 1A) consistently produce stronger MR immunoreactivity in MNCs than do Wistar rats (Fig. 1B). Because this characteristic of WKY rats would allow us to obtain excellent MR immunocytochemical images even in brain sections that were processed for *in situ* hybridisation, we compared the MR expression in the SON and PVN between WKY rats and Wistar rats. Although the distribution of MR-immunoreactivity in WKY rats was similar, if not identical, to that of Wistar rat, the intensity of the labelling in the SON and PVN measured as the optical density (OD) from WKY rats was significantly greater than that from Wistar rats (Fig. 1E). In addition, semi-quantitative RT-PCR showed significantly greater expression of MR in the SON of WKY rats than those of Wistar rats (Fig. 1F). Immunocytochemical localisation of MR was also performed on the sections from the kidney (Fig. 1G) in which the localisation of MR is well established (45–48). In the kidney cortex, an intense MR immunoreactivity was present in the tubules where the cellular morphology and location resembles that of the distal tubules. In the kidney medulla, a strong 11β-HSD2 immunoreactivity was present in collecting ducts.

Double-immunofluorescence confocal microscopy was also employed to exam whether MR is expressed in both VP and OT synthesising MNCs in WKY rats (Fig. 2) as observed previously in Sprague–Dawley rats (9). MR-immunoreactive MNCs were homogeneously located throughout the SON, although the intensity of the immunoreactivity varied among the MNCs (Fig. 2A,D). By contrast, the characteristic distribution of VP and OT neurones was observed. VP immunoreactive neurones were more prevalent in the posterior–ventral region of the nucleus (Fig. 2B), whereas OT immunoreactive neurones were more predominantly located in the anterior–dorsal region (Fig. 2E). Close observation revealed that all VP or OT immunoreactive MNCs were also immunoreactive to MR as well (Fig. 2C,F). In the PVN, MR-immunoreactive neurones of varying intensities were populated in the posterior magnocellular subdivision (Fig. 2G,J). Immunocytochemical localisation of the VP and OT also displayed the stereotypical distribution of VP and OT neurones in the PVN. VP neurones were concentrated in the posterior magnocellular subdivision (Fig. 2H), whereas oxytocin neurones were populated in the area surrounding the posterior magnocellular subdivision (Fig. 2K). As in the SON, all VP and OT immunoreactive MNCs were also immunoreactive to MR in the PVN (Fig. 2I,L).

Localisation of 11β-HSD2 immunoreactivity in the hypothalamus

The 11β-HSD2 antibody labelled essentially all neuronal nuclei in the brain sections. Although this ubiquitous nuclear labelling was proba-

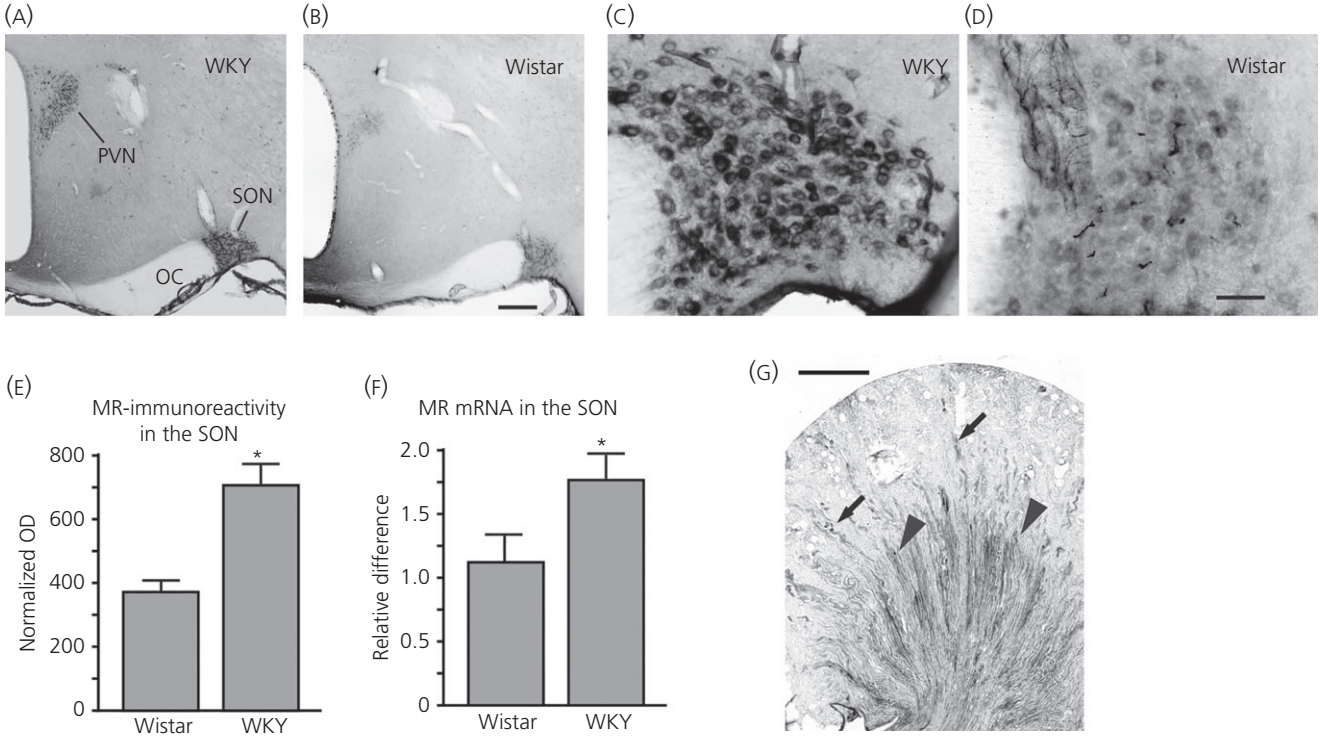

Fig. 1. Immunocytochemical localisation of mineralocorticoid receptor (MR) in coronal section of the hypothalamus from Wistar–Kyoto (WKY) and Wistar rats. (A, B) Prominent MR-immunoreactive neurones were observed only in the supraoptic nucleus (SON) and paraventricular nucleus (PVN) within the hypothalamic region in both WKY rats (A) and Wistar rats (B). (C, D) MR-immunoreactivity in the SON from a WKY rat (C) and a Wistar rat (D). (E) The intensity of the MR-labelling in the SON and PVN was measured as the optical density (OD) and normalised to OD values of nonspecific staining areas outside the SON or PVN. The mean normalised OD value of the SON from WKY rats was significantly higher than that from Wistar rats ($n = 6$ for both strains; $^*P = 0.0021$). (F) Relative expression of MR-mRNA in the SON and PVN was significantly higher in WKY rats than in Wistar rats ($n = 6$ for both strains; $^*P = 0.0271$). (G) Immunocytochemical localisation of MR was also performed in the kidney. An intense MR immunoreactivity was present in the tubules where the cellular morphology and location resembles that of the distal tubules of the kidney cortex (arrows). In the kidney medulla, a strong 11β-hydroxysteroid dehydrogenase type 2 immunoreactivity was present in collecting ducts (arrowheads). OC, optic chiasm. Scale bar = 250 μm in (B), 50 μm in (D) and 1 mm in (G).

bly a result of nonspecific labelling, at a lower power view, the immunoreactivity was most dense in the PVN and SON (Fig. 3A). At higher power views, 11β-HSD2 immunoreactivity was specifically observed in the cytoplasm of the MNCs in the SON (Fig. 3B). In the PVN, cytoplasmic immunoreactivities appeared to be confined to the soma of MNCs in the posterior magnocellular cluster (Fig. 3C). Brain sections obtained from the rats used for MR immunocytochemistry were also treated with the 11β-HSD2 antibody. No noticeable differences were evident in the staining intensities between the rat strains (data not shown). The 11β-HSD2 antibody was also tested on the sections from the kidney (Fig. 3E), which is known to express 11β-HSD2 (44,49). In the kidney cortex, an intense 11β-HSD2 immunoreactivity was present in the tubules, for which the cellular morphology and location resemble that of the distal tubules. In the kidney medulla, a strong 11β-HSD2 immunoreactivity was present in collecting ducts. The expression pattern of the 11β-HSD2 in the kidney was comparable to that characterised in previous studies (44,49).

In situ hybridisation of 11β-HSD2 in the hypothalamus

In situ hybridisation with a labelled antisense RNA probe was used to localise a specific 11β-HSD2 mRNA in the hypothalamus. Although weak ubiquitous labelling of cell nuclei was observed elsewhere in the brain section, prominent hybridisation labelling in the cytoplasm was seen only in the PVN and SON (Fig. 4A). Within the PVN, labelling showed the well characterised 'butterfly wing' shape with more prominent labelling in the posterior magnocellular region; however, noticeable labelling was also observed in the parvocellular regions as well (Fig. 4B). Somewhat more discrete cytoplasmic labelling was found in the SON (Fig. 4C). The sense probe that was processed in parallel with the experimental brain sections did not produce any detectable labelling (Fig. 4D). In addition, *in situ* hybridisation of 11β-HSD2 was performed on the kidney sections. The expression pattern of the *in situ* labelling in the kidney resembled that of the immunoreactivity (i.e. the intense hybridisation labelling was present in the tubules where the cellular morphology and location resembles that of the distal tubules of the kidney cortex). Also, strong hybridisation labelling was present in collecting ducts in the kidney medulla.

Co-localisation of MR and 11β-HSD2 in MNCs of the SON and PVN

11β-HSD2 *in situ* hybridised sections were subsequently processed for MR immunocytochemistry using a double-fluorescent labelling

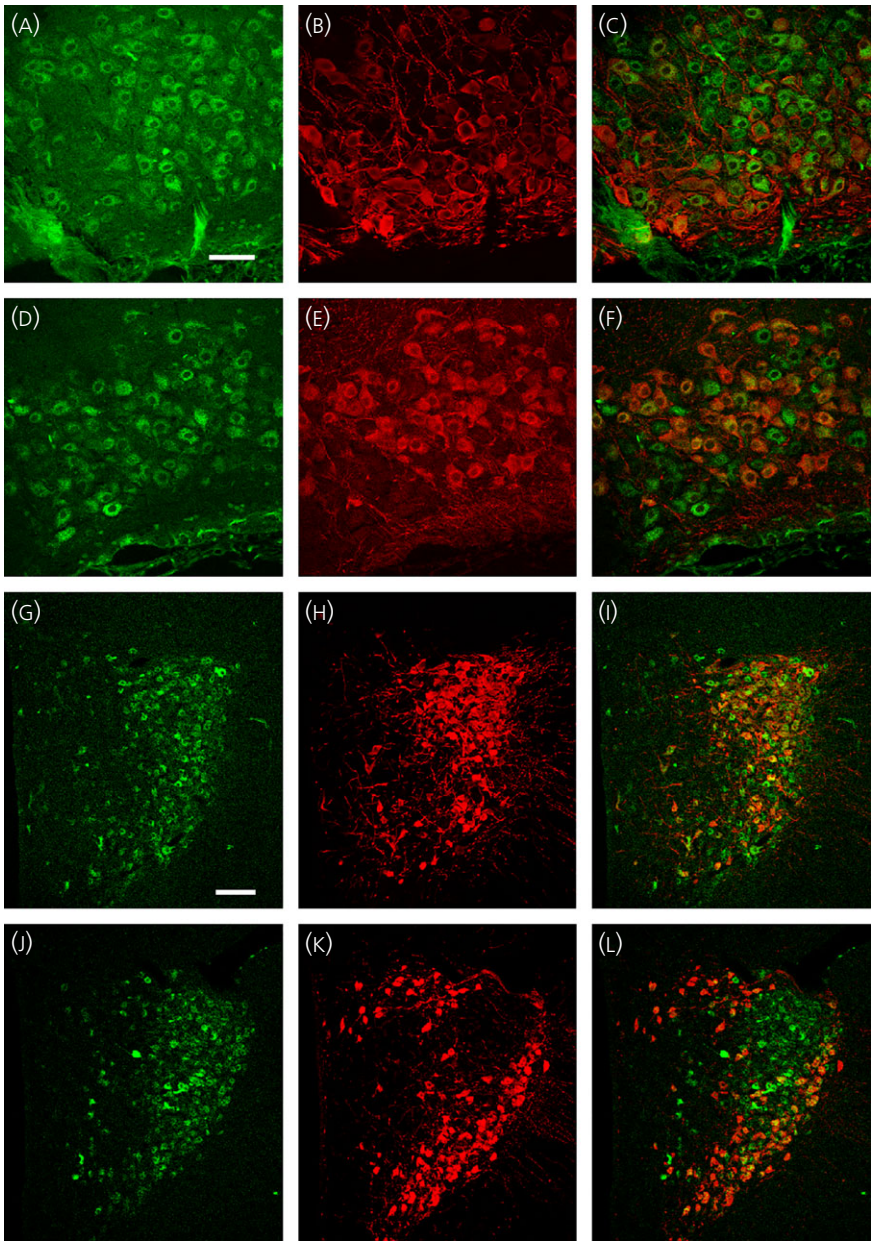

Fig. 2. Colocalisation of mineralocorticoid receptor (MR) immunoreactivity with both vasopressin (VP)-neurophysin (NP) and oxytocin (OT)-NP immunoreactivity in the supraoptic nucleus (SON) and paraventricular nucleus (PVN) from a Wistar–Kyoto (WKY) rat. All confocal photomicrographs are in a coronal 3-μm optical section. MR-immunoreactivity was labelled with DyLight 488-conjugated secondary antibody (pseudo-coloured in green). VP-NP and OT-NP immunoreactivities were labelled with DyLight 649-conjugated secondary antibody (pseudo-coloured in red). (A, D) MR-immunoreactivity in the SON. Most magnocellular neurosecretory cells (MNCs) in the SON appeared to possess some degree of MR-immunoreactivity in their cell bodies. (B) VP-NP immunoreactivity in the same section and optical plane as in (A). (C) A merged image of (A) and (B) demonstrated that all the VP-NP immunoreactive MNCs retain MR-immunoreactivity. (E) OT-NP immunoreactivity in the same section and image plane as in (D). (F) A merged image of (D) and (E) demonstrated that all OT-NP immunoreactive MNCs possess MR immunoreactivity. (G, J) MR-immunoreactivity in the PVN. Although the MR-immunoreactivity was not robust as in the SON, a prominent MR immunoreacitivty was observed in MNC within the PVN. Most of these MR-immunoreactive MNCs are located in a cluster of cells in the posterior magnocellular region. (H) VP-NP immunoreactivity in same section and image plane as in (G). Note that the VP-NP immunoreactive cells form a cluster in the lateral portion of the PVN. (I) A merged image of (G) and (H) showed that all VP-NP immunoreactive MNCs expressed MR-immunoreactivity. (K) OT-NP immunoreactivity in same section and image plane as in (J). (L) Merged images of (J) and (K) revealed that MR-immunoreactivity is colocalised with OT-NP immunoreactivity within MNCs in the PVN. Scale bar = 50 μm in (A) and 100 μm in (G).

technique with confocal microscopy. Several WKY rats were used for this because robust MR-immunoreactivity remained following *in situ* hybridisation in the PVN (Fig. 5A) and SON (Fig. 5D). All MR-immunoreactive MNCs had 11β-HSD2 hybridisation labelling in the PVN (Fig. 5B,C) and SON (Fig. 5E,F). Confocal images at 1 μm optical sections acquired with a × 100 objective lens allowed us to

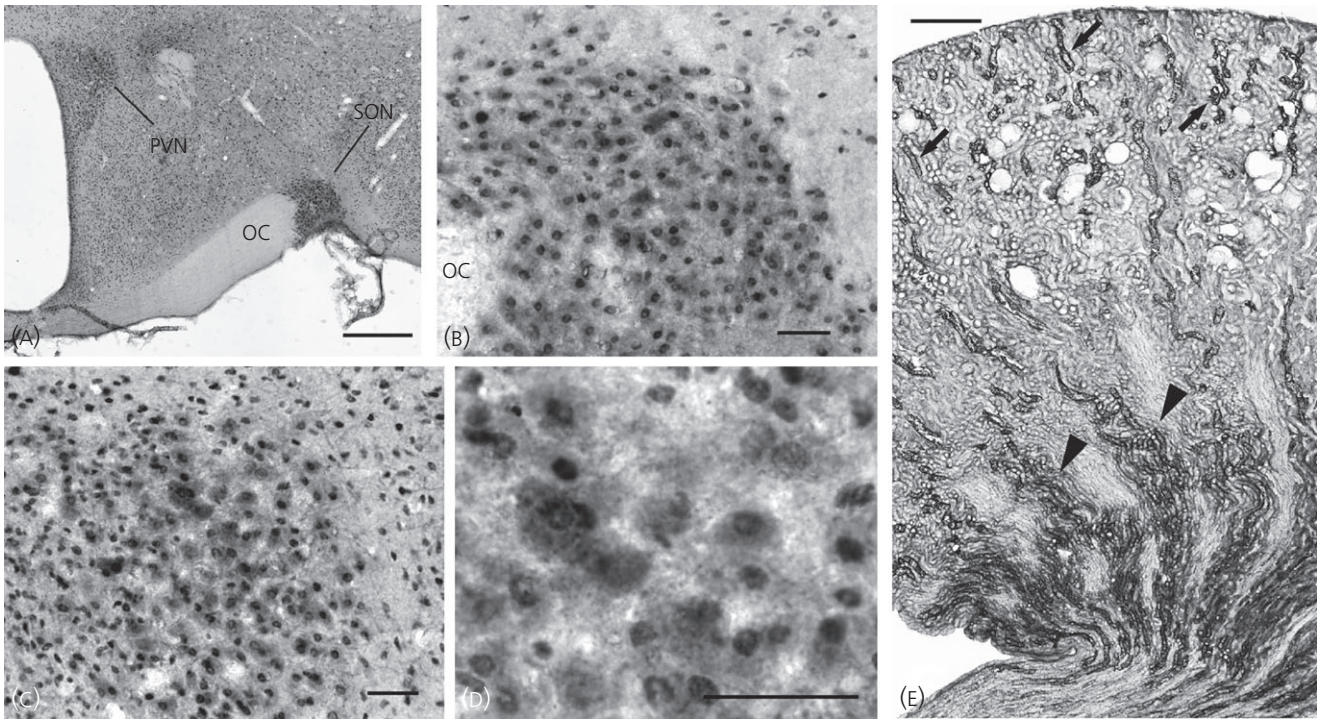

Fig. 3. Immunocytochemical localisation of 11β-hydroxysteroid dehydrogenase type 2 (11β-HSD2) in sections of the hypothalamus and kidney from a Wistar–Kyoto (WKY) rat. (A) 11β-HSD2 immunoreactivity was observed in essentially all neuronal nuclei in the brain section. This ubiquitous nuclear labelling was most likely nonspecific labelling; however, the immunoreactivity was dense in the paraventricular nucleus (PVN) and supraoptic nucleus (SON). (B) In the SON, magnocellular neurosecretory cells (MNCs) containing cytoplasmic immunoreactivity were observed. Note that cells outside of the SON are devoid of cytoplasmic immunoreactivity. (C) In the PVN, the cells possessing cytoplasmic immunoreactivity were mostly located in the posterior magnocellular cluster. (D) A higher power view demonstrates cytoplasmic immunoreactivity in MNCs in the PVN. (E) Immunocytochemical localisation of 11β-HSD2 was also performed in the kidney. In the kidney cortex, an intense 11β-HSD2 immunoreactivity was present in the tubules for which the cellular morphology and location resemble that of the distal tubules (arrows). In the kidney medulla, a strong 11β-HSD2 immunoreactivity was present in collecting ducts (arrowheads). OC, optic chiasm. Scale bar = 500 μm in (A) and (E), 50 μm in (B–D).

observe the subcellular distribution of 11β-HSD2 hybridisation labelling and MR immunoreactivity. Immunoreactivity to MR was observed demonstrating a distinct granular appearance clumped in the perinuclear zone of the cytoplasm, although immunoreactivity was also observed diffusely within the entire cytoplasm (Fig. 5G). By contrast, 11β-HSD2 hybridisation labelling was stronger in the peripheral region of the cytoplasm (Fig. 5H). A merged image demonstrated a subcellular distribution difference of MR immunoreactivity and 11β-HSD2 hybridisation labelling (Fig. 5I).

Single-cell RT-PCR detection of MR and 11β-HSD2 mRNA

Seventy-five dissociated cells were collected individually from three Wistar rats and three WKY rats. Typically, 12–15 cells were harvested from each animal. Following total RNA extraction and reverse-transcription from these single cells, PCR for VP and OT were performed. Either or both VP- and OT-mRNA were detected from all dissociated neurones, confirming that the collected cells were MNCs. Co-localisation of OT- and VP-mRNA was found in most MNCs. Several other studies also demonstrated the co-localisation of both mRNAs in MNCs even though they are phenotypically different (50–52). Because our assay was not quantitative, the absolute levels of OT- and VP-mRNAs are unknown and therefore the phenotypes of the MNCs were not defined. cDNA from each MNC was amplified by PCR for MR and 11β-HSD2. Out of seventy-five MNCs, amplified products of expected sizes for MR and 11β-HSD2 were obtained from fifty-six (74.7%) and twenty-four (32.0%) MNCs, respectively. Of fifty-six MNCs expressing MR, twenty-one (37.5%) MNCs also expressed 11β-HSD2. The incidence of MR and 11β-HSD2 co-expression did not differ significantly among individual rats or between strains. Representative single-cell RT-PCR gel images from a WKY rat are shown in Fig. 6.

Discussion

Expression of MR in the SON and PVN of the WKY rat

The present study demonstrated that the expression of MR in the SON and PVN is greater in WKY rats than in Wistar rats. We determined that MR is expressed in both VP and OT MNCs in WKY rats in accordance with our previous finding in Sprague–Dawley rats (9,16–19). Because *in situ* hybridisation caused an increase in background staining in immunocytochemistry at the same time as diminishing specific MR-immunolabelling, double-labelling of 11β-

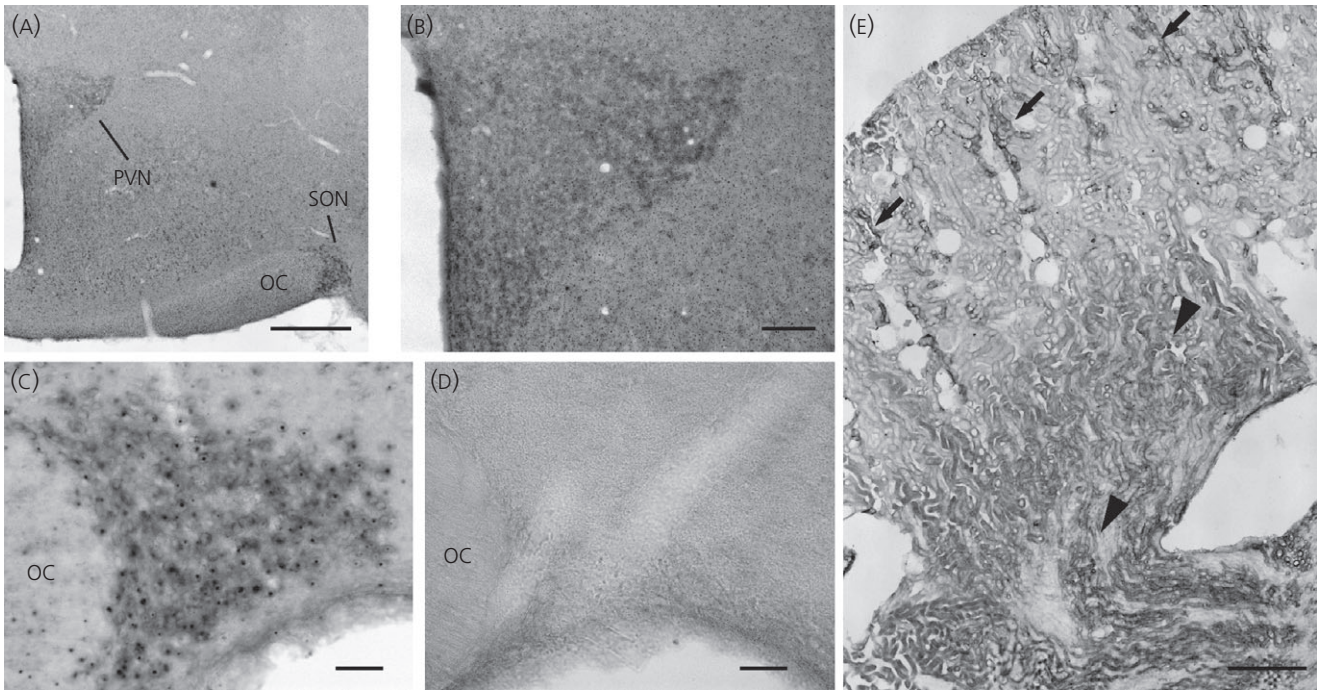

Fig. 4. *In situ* hybridisation detection of 11β-hydroxysteroid dehydrogenase type 2 (11β-HSD2) mRNA in the hypothalamus of a Wistar–Kyoto (WKY) rat. (A) Weak ubiquitous labelling of cell nuclei was observed elsewhere in the brain section; however stronger hybridisation labelling was seen in the paraventricular nucleus (PVN) and supraoptic nucleus (SON) in which cytoplasmic labelling were present in neurones. (B) Within the PVN, more prominent cytoplasmic labelling was observed in the posterior magnocellular region; however, noticeable cytoplasmic labelling was also observed in the parvocellular regions as well. (C) Discrete cytoplasmic labelling was found in magnocellular neurosecretory cells (MNCs) in the SON. (D) The sense probe that was processed in parallel with the experimental bran sections did not produce detectable labelling in the SON. (E) *In situ* hybridisation of 11β-HSD2 was also performed in the kidney. The expression pattern of the *in situ* labelling in the kidney was resembled to that of immunoreactivity (Fig. 3E). An intense hybridisation labelling was present in the distal tubules in the cortex (arrows) and in the collecting ducts in the medulla region (arrowheads). OC, optic chiasm. Scale bar = 500 μm in (A), 100 μm in (B), 50 μm in (C) and (D), and 1 mm in (E).

HSD2 *in situ* hybridisation and MR immunocytochemistry was particularly challenging. As a result of the higher expression of hypothalamic MR in WKY rats, obtaining decent images of MR immunolabelling in 11β-HSD2 *in situ* hybridised brain sections became possible. Thus, the WKY strain is an amenable strain for investigating the co-localisation of MR and11β-HSD2 in MNCs.

The WKY rat is a normotensive back strain of the spontaneously hypertensive rat (SHR), which is a well-studied animal model of human essential hypertension (53). Thus, WKY rats have been used as appropriate control for SHR. A recent report showed that the SHR strain has an elevated hypothalamic MR mRNA, as well as an increased number of MR-immunopositive cells in the magnocellular paraventricular region, compared to that from WKY rats (20). The increased expression of MR in the PVN of SHR rats most likely contributes to the development of hypertension because i.c.v. infusion of the MR-antagonist caused a significant decrease in blood pressure (20). An intriguing point is that the normotensive WKY rats have already considerably greater MR expression in the SON and PVN compared to another normotensive Wistar rats. Thus, SHR that reportedly have even greater hypothalamic MR expression was developed for higher blood pressure by selective breeding of the WKY stock (53), which already has elevated hypothalamic MR-expression.

11β-hydroxysteroid dehydrogenase activity in the hypothalamus

The present study investigates whether the glucocorticoid-inactivating enzyme, 11β-HSD2, is located in MR expressing MNCs in the hypothalamic SON and PVN. Double-immunocytochemistry showed that all MR immunoreactive neurones were also immunoreactive to VP or OT. Double-labelling using immunocytochemistry and *in situ* hybridisation demonstrated that all MR immunoreactive MNCs were also labelled with11β-HSD2 *in situ* hybridisation. Although MR and 11β-HSD mRNAs were not detected in all harvested MNCs in single-cell RT-PCR, MR and 11β-HSD2 mRNAs were detected in 74.7% and 32% of harvested MNCs, respectively. Moreover, 11β-HSD2 mRNA was detected in 37.5% of MR expressing MNCs identified by single-cell RT-PCR. Failure to detect MR and 11β-HSD2 mRNA in all cells with single-cell RT-PCR was probably a result of the minute amount of the mRNAs that may be ruined during the process in some cells rather than the absence of the mRNAs. Based on our past single-cell RT-PCR assays (9,54), it is rare to detect certain mRNA from every single MNC unless the mRNA is expressed abundantly such as VP and OT mRNAs. Nonetheless, our findings strongly suggest that MR-expressing VP and OT MNCs also express 11β-HSD2. The co-localisation of MR and 11β-HSD2 in MNCs

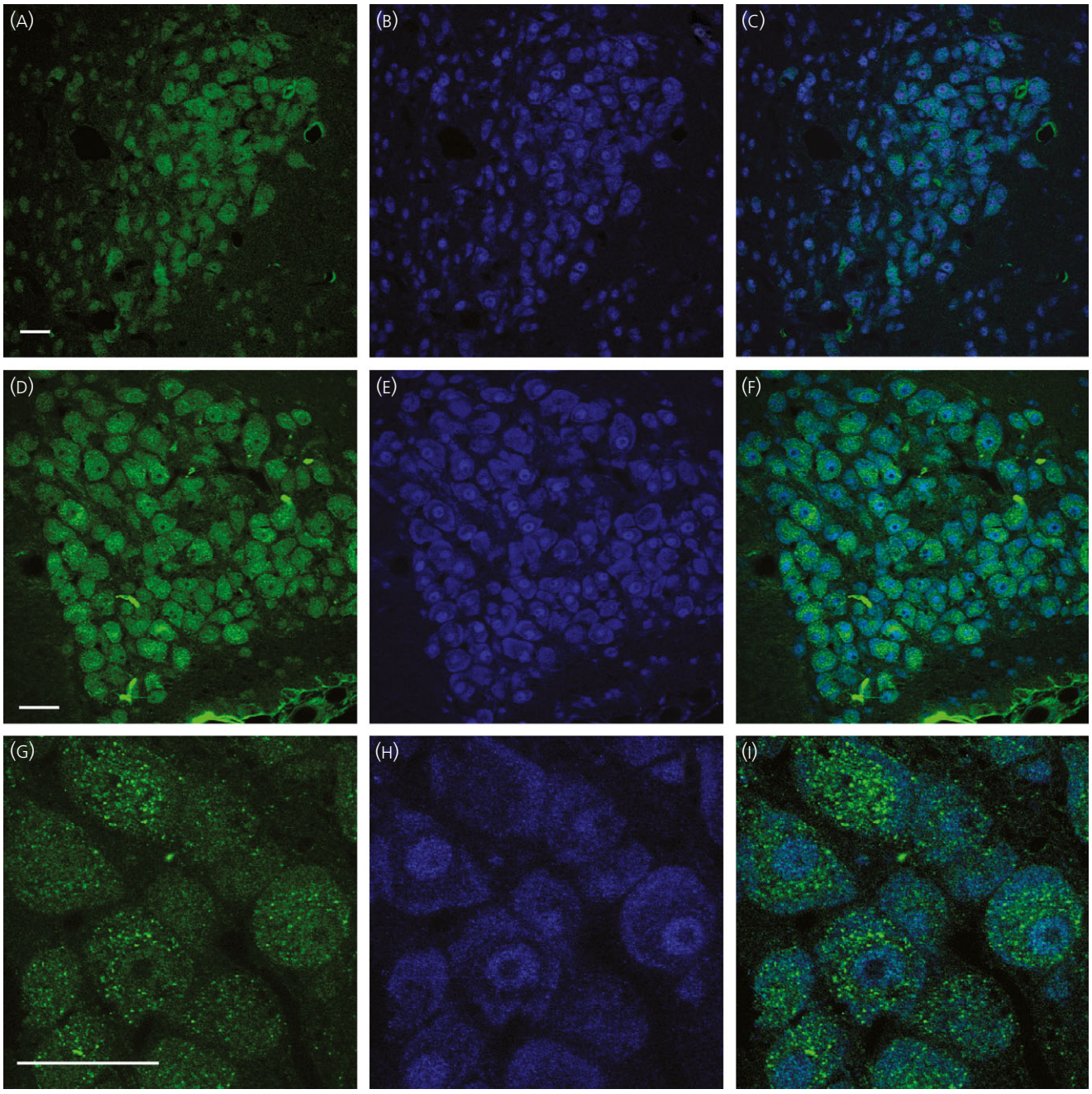

Fig. 5. Double fluorescent labelling of 11β-hydroxysteroid dehydrogenase type 2 (11β-HSD2) *in situ* hybridisation and mineralocorticoid receptor (MR) immunocytochemistry. MR immunoreactivity was labelled with DyLight 488-conjugated secondary antibody (pseudo-coloured in green). (A, D) Intense immunoreactivity to MR was observed in the MNCs in the paraventricular nucleus (PVN) (A) and supraoptic nucleus (SON) (D). (B, E) 11β-HSD2 hybridisation materials were labelled with DyLight 649-conjugated secondary antibody (pseudo-coloured in blue) in same section and image plane as in (A) and (D). The 11β-HSD2 hybridisation materials were observed in the magnocellular neurosecretory cells (MNCs) in the PVN (B) and SON (E). (C, F) The merged images revealed that all MR immunoreactivity was co-localised with vasopressin (VP) 11β-HSD2 hybridisation materials within the MNCs in the PVN (C) and SON (F). (G, H) Confocal images at 1 μm optical section acquired with a × 100 objective lens were obtained to observe the subcellular distribution of MR immunoreactivity (G) and 11β-HSD2 hybridisation labelling (H) in the SON MNCs. Intense MR immunoreactivity was clumped in the perinuclear zone of the cytoplasm with a distinct granular appearance along with more diffuse immunoreactivity within the entire cytoplasm (G). Strong 11β-HSD2 hybridisation labelling was observed in the peripheral region of the cytoplasm (H). (I) A merged image demonstrated that MR immunoreactivity was co-localised with 11β-HSD2 hybridisation product in MNCs, although their subcellular distributions were different from each other. Scale bars = 50 μm.

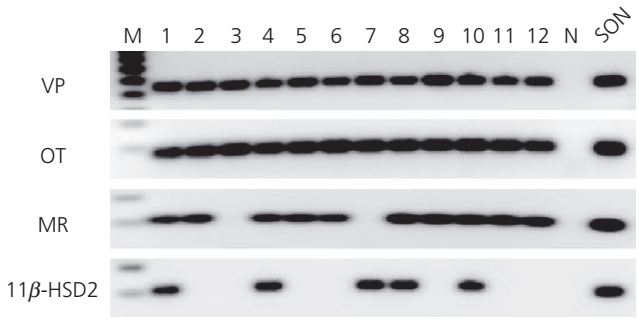

Fig. 6. Single cell reverse transcriptase-polymerase chain reaction detection of transcripts in individual dissociated magnocellular neurosecretory cells (MNCs) from a Wistar–Kyoto (WKY) rat. Libraries of cDNA were derived from twelve cells dissociated from punched supraoptic nucleus (SON) tissue from a WKY rat. All cells had mRNA for vasopressin (VP) and oxytocin (OT), confirming they were MNCs. Of these MNCs, mineralocorticoid receptor (MR) mRNA was found in MNCs except #3 and 7; 11β-hydroxysteroid dehydrogenase type 2 (11β-HSD2) mRNA was found in cells #1, 4, 7, 8 and 10. Thus, mRNAs for MR and 11β-HSD2 were colocalised in four MNCs (#1, 4, 8 and 10) out of 12 MNCs isolated. Both MR and 11β-HSD2 mRNAs were found in cDNA library derived from punched SON tissues. M, Marker; N, Negative control.

suggests further that MNCs in the SON and PVN are aldosterone-sensitive neurones.

The presence of an hydroxyl group at position C-11 of the steroid structure of glucocorticoids is important for its biological activity because conversion of this group into a keto group inactivates the steroid (55). The principal glucocorticoids, cortisol in human and corticosterone in rodents, possess a hydroxyl group at C-11 and are active steroids. Conversion of the C-11 hydroxyl group into a keto group of cortisol and corticosterone results in the conversion of these active steroids into inactive cortisone and 11-dehydrocorticosteone, respectively. Two microsomal isozymes of 11β-hydroxysteroid dehydrogenase, 11β-HSD1 and 11β-HSD2, are known to catalyze this conversion, and tissue-specific expression of these isozymes promote pre-receptor regulation of glucocorticoid and mineralocorticoid receptor activation (56).

Activity of 11β-HSD is documented in the hypothalamus. A prominent formation of 11-dehydrocorticosterone from corticosterone was observed in incubated hypothalamic minces from rats (57). Moreover, microinjection of the 11β-HSD inhibitors, carbenoxolone or glycyrrhizic acid, directly into the PVN caused an increase in mean arterial pressure, heart rate and renal sympathetic nerve activity (35). The inhibition of 11β-HSD likely permitted corticosterone to activate MRs because i.c.v. infusion of the MR antagonist, spironolactone, blocked the effect of the 11β-HSD inhibitors (35). However, these findings did not confirm whether the dehydrogenase activity was a result of 11β-HSD1 or to 11β-HSD2.

By contrast to 11β-HSD2, which has a limited expression, 11β-HSD1 is abundantly expressed throughout the brain (58–61) including the PVN (41). Unlike 11β-HSD2, which exclusively catalyses the hydroxysteroid dehydrogenase activity that converts biologically active glucocorticoids into biologically inactive metabolites, 11β-HSD1 is a bidirectional enzyme that also mediates the reverse reaction; keto-glucorticoid reductase activity converts inactive metabolites into potent glucocorticoids (62–65). The direction of the enzymatic activities depends upon the availability of the cofactors, the oxidised/reduced forms of nicotinamide adenine dinucleotide phosphate ($NADP^+$/NADPH). The reductase activity of 11β-HSD1 requires NADPH as a cofactor, whereas its dehydrogenase activity requires $NADP^+$ (29). The production of NADPH requires another microsomal enzyme, hexose-6-phosphate dehydrogenase (H6PDH), which catalyzes glucose-6-phosphate oxidation to generate NADPH from $NADP^+$ for 11β-HSD1 in the endoplasmic reticulum lumen (66). Thus, in the absence of H6PDH, 11β-HSD1 uses $NADP^+$ and primarily acts as a dehydrogenase (66–69). Recently, colocalisation of MR and 11β-HSD1 immunoreactivities was reported in some identified preautonomic neurones in the PVN. Because no immunoreactivity to H6PDH was found in these MR-11β-HSD1 immunoreactive neurones, it is proposed that 11β-HSD1 in the preautonomic neurones acts mainly act as a dehydrogenase and facilitates the binding of aldosterone to MR (41). The same study also demonstrated the presence of 11β-HSD1 immunoreactivity in MNCs of the PVN. Although the study did not specifically address the colocalisation of 11β-HSD1 and MR in MNCs, the absence of H6PDH immunoreactivity in the PVN implies that 11β-HSD1 may act as a dehydrogenase in MNCs in the PVN.

Previous studies demonstrated that 11β-HSD2 is located to the membrane of the endoplasmic reticulum (ER) with its active site and co-factor binding domain facing the cytosol (70) where aldosterone is presumably located, and binds to its substrate with an affinity approximately 100 times that of 11β-HSD1 (71–73). By contrast, the intracellular localisation of 11β-HSD1 is located within the lumen of the ER where H6PDH may generate NADPH (70), which may explain why 11β-HSD1 acts as a reductase in most cells unless the cells are disrupted (56). Consequently, if the two enzymes are co-expressed, the higher binding affinity of 11β-HSD2 to the substrate and the specific intracellular localisation of 11β-HSD2 result in 11β-HSD2 playing a more dominant role in corticosteroid metabolism in tissues (56). Thus, these findings suggest that a limited amount of 11β-HSD2 suffices to protect MR from glucocorticoids in the MNCs.

Possible roles of MR-mediated aldosterone in MNCs

The effect on blood pressure of MR-mediated aldosterone in the brain is well-established by a number of studies (74–76). Many of these studies involved i.c.v. infusion of aldosterone and/or specific MR blockers, and demonstrated that aldosterone activation of MR in the brain increases release of VP and blood pressure via enhancing the sympathetic drive to the kidney, heart and vascular smooth muscle (77–79). Intriguingly, i.c.v. infusion of ENaC blockers, amiloride or benzamil, prevented both the hypertension induced by i.c.v. infusion of aldosterone in SD rats (80) and the salt-induced hypertension in Dahl-salt-sensitive (SS) rats (81,82). Although these studies provide only limited information regarding brain site(s) or cell type(s) responsible for the MR-mediated aldosterone action, their findings indicate that brain structures expressing MR, 11β-HSD2 and ENaC not only have the ability to modulate sympathetic drive and VP release, but also are the sites for aldosterone action.

Expression of MR in the brain was previously documented in the choroid plexus, ependyma, neurones in the SON and PVN, the nucleus tractus solitarius and in the subfornical organ (9,16,18,40,83). Of these MR-expressing structures, both mRNA and proteins for all three ENaC subunits (α, β, and γ) were found in MNCs of the SON and PVN, choroid plexus, and ependyma (9,16,18,40,83). Of the brain structures that express MR and ENaC, the SON and PVN are the only brain structures that directly affect both neuroendocrine (VP release) and autonomic responses in the regulation of blood pressure. However, the mechanism of how aldosterone-MR influences the activity of the MNCs is unknown.

Previously, we demonstrated that ENaCs in MNCs mediate a Na^+ leak current and modulate the membrane potential (84) that affect the frequency and pattern of action potentials. Because the release of neurohypophysial hormones largely depends upon the neuronal activity of MNCs (2,10) and because somato-dendritic release of VP within the PVN affects presympathetic neurones (8), we proposed a novel theoretical concept where ENaCs modulate the frequency of action potentials in MNCs that modulate neuroendocrine and autonomic responses, which, in turn, contribute to cardiovascular homeostasis.

In aldosterone-sensitive epithelia of the kidney, the activation of MR by aldosterone not only regulates gene expression of ENaC subunits (11–15), but also a variety of genes, including those for regulatory proteins for ENaCs. The serum- and glucocorticoid-inducible kinase 1 (SGK1) is one of the ENaC regulatory proteins that is also promoted by aldosterone-MR activation (85,86). The effects of SGK1 on ENaC activity were extensively studied in aldosterone-sensitive epithelia. Activated SGK1 directly increased α-ENaC transcription (87,88), disrupted ENaC internalisation from the cell membrane (89–91) and increased channel open probability (92). Because SGK1 is expressed in the SON and PVN of the rat brain (34), multiple levels of regulation, synthesis and translocation of ENaC by MR likely occur in MNCs.

Dietary salt intake is known to affect the production and release of the sodium-retaining hormone, aldosterone, from the adrenal cortex (93–95). Plasma aldosterone concentrations are low in rats maintained on a normal or high-salt diet. By contrast, the plasma concentration of aldosterone increased in rats maintained on a low-salt diet. Aldosterone concentration in the hypothalamus is also affected by dietary salt intake. However, the concentration of aldosterone in the hypothalamus in Dahl-SS rats reportedly increased, not decreased, with high dietary salt intake (82,96,97). In addition, i.c.v. infusion of Na^+-rich artificial CSF caused an increase in hypothalamic aldosterone concentration and blood pressure (98). Importantly, the increase in both hypothalamic aldosterone and blood pressure was prevented by i.c.v. infusion of an aldosterone synthase inhibitor (98). These results suggest that, in response to elevated Na^+ concentration in the CSF or increased dietary salt intake, aldosterone is synthesised in the hypothalamus independent of the adrenal cortex. Transcripts of aldosterone synthase, CYP11B2, were detected in various brain regions including the hypothalamus (99). Moreover, SS hypertension in Dahl-SS rats is alleviated by central infusion of several inhibitors of steroid synthesis, including one specific for aldosterone synthase (68,96). Local aldosterone synthesis suggests that there may be sufficient aldosterone concentrations in the immediate vicinity of MR-expressing MNCs that would result in elevated binding of aldosterone on MRs in the MNCs. Thus, a large amount of 11β-HSD2 may not be necessary in the MNCs of the SON and PVN.

Dietary salt intake is also known to be affected by aldosterone. Several studies showed that aldosterone induces salt appetite when its release is increased in response to sodium deficiency (100–103). Aldosterone induces sodium appetite through MR in the brain because infusion of aldosterone into the fourth ventricle alone resulted in increased sodium appetite, which was blocked by an MR antagonist (104). One of the potential brain areas mediating the aldosterone induced sodium appetite is the MR and 11β-HSD2 co-expressing neurones in the nucleus tractus solitarius (40). By contrast, several studies have demonstrated that centrally released OT mediates the inhibition of sodium appetite (105–109), whereas OT release into the general circulation does not appear to be involved in the inhibition of sodium appetite (110). Interestingly, treatment with a precursor of aldosterone, deoxycorticosterone acetate, caused a decrease in neuronal activity of OT neurones in the SON and PVN (111–113). Thus, the presence of MR and 11β-HSD2 in OT neurones implies that aldosterone directly inhibits these neurones via the MR. The inhibitory effect of aldosterone on OT neurone may be necessary during hypernatraemia, the condition known to decrease sodium appetite (105,114–116). Because the sodium concentration in the cerbrospinal fluid (CSF) is elevated during hypernatraemia (117) and a high concentration of sodium in CSF causes an increase in hypothalamic aldosterone concentration (98), inhibition of sodium appetite caused by the elevated CSF sodium concentration (114,118,119) may be mediated by the central aldosterone via MR in OT neurones.

Conclusions

The present study demonstrates that the glucocorticoid-inactivating enzyme, 11β-HSD2, is located in MR expressing OT and VP MNCs in the SON and PVN. These findings strongly suggest that MR in MNCs are mostly regulated by aldosterone. Considering the roles of VP and OT in the fluid/electrolyte balance, the colocalisation of MR and 11β-HSD2 suggests that the effect of central aldosterone on blood pressure is mediated, at least partly, via MR in MNCs.

Acknowledgements

The present study was supported by National Heart, Lung, and Blood Institute Grant R01 HL115208 (R. Teruyama). The authors thank Dr. J. T. Caprio for reading earlier versions of this article and L. L. Wilson and N. E. J. Wandrey for technical assistance.

Received 1 June 2015,
revised 15 September 2015,
accepted 17 September 2015

References

1 Sladek CD. Antidiuretic Hormone: Synthesis and Release. *Handbook of physiology, Section 7*. 2000; The Endocrine System (Endocrine Regulation of Water and Electrolyte Balance). Oxford: Oxford University Press.
2 Poulain DA, Wakerley JB. Electrophysiology of hypothalamic magnocellular neurones secreting oxytocin and vasopressin. *Neuroscience* 1982; **7**: 773–808.
3 Verbalis JG. The brain oxytocin receptor(s)? *Front Neuroendocrinol* 1999; **20**: 146–156.
4 Huang W, Lee SL, Sjoquist M. Natriuretic role of endogenous oxytocin in male rats infused with hypertonic NaCl. *Am J Physiol* 1995; **268**: R634–R640.
5 Crowley WR, Armstrong WE. Neurochemical regulation of oxytocin secretion in lactation. *Endocr Rev* 1992; **13**: 33–65.
6 Bourque CW. Central mechanisms of osmosensation and systemic osmoregulation. *Nat Rev Neurosci* 2008; **9**: 519–531.
7 Toney GM, Stocker SD. Hyperosmotic activation of CNS sympathetic drive: implications for cardiovascular disease. *J Physiol* 2010; **588**: 3375–3384.
8 Son SJ, Filosa JA, Potapenko ES, Biancardi VC, Zheng H, Patel KP, Tobin VA, Ludwig M, Stern JE. Dendritic peptide release mediates interpopulation crosstalk between neurosecretory and preautonomic networks. *Neuron* 2013; **78**: 1036–1049.
9 Teruyama R, Sakuraba M, Wilson LL, Wandrey NE, Armstrong WE. Epithelial Na(+) sodium channels in magnocellular cells of the rat supraoptic and paraventricular nuclei. *Am J Physiol Endocrinol Metab* 2012; **302**: E273–E285.
10 Cazalis M, Dayanithi G, Nordmann JJ. The role of patterned burst and interburst interval on the excitation- coupling mechanism in the isolated rat neural lobe. *J Physiol* 1985; **369**: 45–60.
11 Masilamani S, Kim GH, Mitchell C, Wade JB, Knepper MA. Aldosterone-mediated regulation of ENaC alpha, beta, and gamma subunit proteins in rat kidney. *J Clin Invest* 1999; **104**: R19–R23.
12 Renard S, Voilley N, Bassilana F, Lazdunski M, Barbry P. Localization and regulation by steroids of the alpha, beta and gamma subunits of the amiloride-sensitive Na^+ channel in colon, lung and kidney. *Pflugers Arch* 1995; **430**: 299–307.
13 Escoubet B, Coureau C, Bonvalet JP, Farman N. Noncoordinate regulation of epithelial Na channel and Na pump subunit mRNAs in kidney and colon by aldosterone. *Am J Physiol* 1997; **272**: C1482–C1491.
14 Stokes JB, Sigmund RD. Regulation of rENaC mRNA by dietary NaCl and steroids: organ, tissue, and steroid heterogeneity. *Am J Physiol* 1998; **274**: C1699–C1707.
15 MacDonald P, MacKenzie S, Ramage LE, Seckl JR, Brown RW. Corticosteroid regulation of amiloride-sensitive sodium-channel subunit mRNA expression in mouse kidney. *J Endocrinol* 2000; **165**: 25–37.
16 Amin MS, Wang HW, Reza E, Whitman SC, Tuana BS, Leenen FH. Distribution of epithelial sodium channels and mineralocorticoid receptors in cardiovascular regulatory centers in rat brain. *Am J Physiol Regul Integr Comp Physiol* 2005; **289**: R1787–R1797.
17 Ahima R, Krozowski Z, Harlan R. Type I corticosteroid receptor-like immunoreactivity in the rat CNS: distribution and regulation by corticosteroids. *J Comp Neurol* 1991; **313**: 522–538.
18 Han F, Ozawa H, Matsuda K, Nishi M, Kawata M. Colocalization of mineralocorticoid receptor and glucocorticoid receptor in the hippocampus and hypothalamus. *Neurosci Res* 2005; **51**: 371–381.
19 Sanchez MM, Young LJ, Plotsky PM, Insel TR. Distribution of corticosteroid receptors in the rhesus brain: relative absence of glucocorticoid receptors in the hippocampal formation. *J Neurosci* 2000; **20**: 4657–4668.
20 Pietranera L, Brocca ME, Cymeryng C, Gomez-Sanchez E, Gomez-Sanchez CE, Roig P, Lima A, De Nicola AF. Increased expression of the mineralocorticoid receptor in the brain of spontaneously hypertensive rats. *J Neuroendocrinol* 2012; **24**: 1249–1258.
21 Beaumont K, Fanestil DD. Characterization of rat brain aldosterone receptors reveals high affinity for corticosterone. *Endocrinology* 1983; **113**: 2043–2051.
22 Krozowski ZS, Funder JW. Renal mineralocorticoid receptors and hippocampal corticosterone-binding species have identical intrinsic steroid specificity. *Proc Natl Acad Sci USA* 1983; **80**: 6056–6060.
23 Reul JM, de Kloet ER. Two receptor systems for corticosterone in rat brain: microdistribution and differential occupation. *Endocrinology* 1985; **117**: 2505–2511.
24 Sheppard KE, Funder JW. Equivalent affinity of aldosterone and corticosterone for type I receptors in kidney and hippocampus: direct binding studies. *J Steroid Biochem* 1987; **28**: 737–742.
25 de Kloet ER, Van Acker SA, Sibug RM, Oitzl MS, Meijer OC, Rahmouni K, de Jong W. Brain mineralocorticoid receptors and centrally regulated functions. *Kidney Int* 2000; **57**: 1329–1336.
26 Edwards CR, Stewart PM, Burt D, Brett L, McIntyre MA, Sutanto WS, de Kloet ER, Monder C. Localisation of 11 beta-hydroxysteroid dehydrogenase–tissue specific protector of the mineralocorticoid receptor. *Lancet* 1988; **2**: 986–989.
27 Naray-Fejes-Toth A, Watlington CO, Fejes-Toth G. 11 beta-Hydroxysteroid dehydrogenase activity in the renal target cells of aldosterone. *Endocrinology* 1991; **129**: 17–21.
28 Funder JW, Pearce PT, Smith R, Smith AI. Mineralocorticoid action: target tissue specificity is enzyme, not receptor, mediated. *Science* 1988; **242**: 583–585.
29 Agarwal AK, Mune T, Monder C, White PC. NAD(+)-dependent isoform of 11 beta-hydroxysteroid dehydrogenase. Cloning and characterization of cDNA from sheep kidney. *J Biol Chem* 1994; **269**: 25959–25962.
30 Kotelevtsev Y, Brown RW, Fleming S, Kenyon C, Edwards CR, Seckl JR, Mullins JJ. Hypertension in mice lacking 11beta-hydroxysteroid dehydrogenase type 2. *J Clin Invest* 1999; **103**: 683–689.
31 Naray-Fejes-Toth A, Colombowala IK, Fejes-Toth G. The role of 11beta-hydroxysteroid dehydrogenase in steroid hormone specificity. *J Steroid Biochem Mol Biol* 1998; **65**: 311–316.
32 Zhou MY, Gomez-Sanchez EP, Cox DL, Cosby D, Gomez-Sanchez CE. Cloning, expression, and tissue distribution of the rat nicotinamide adenine dinucleotide-dependent 11 beta-hydroxysteroid dehydrogenase. *Endocrinology* 1995; **136**: 3729–3734.
33 Gomez-Sanchez EP, Gomez-Sanchez CM, Plonczynski M, Gomez-Sanchez CE. Aldosterone synthesis in the brain contributes to Dahl salt-sensitive rat hypertension. *Exp Physiol* 2010; **95**: 120–130.
34 Wang HW, Amin MS, El-Shahat E, Huang BS, Tuana BS, Leenen FH. Effects of central sodium on epithelial sodium channels in rat brain. *Am J Physiol Regul Integr Comp Physiol* 2010; **299**: R222–R233.
35 Zhang ZH, Kang YM, Yu Y, Wei SG, Schmidt TJ, Johnson AK, Felder RB. 11beta-hydroxysteroid dehydrogenase type 2 activity in hypothalamic paraventricular nucleus modulates sympathetic excitation. *Hypertension* 2006; **48**: 127–133.
36 Ito K, Hirooka Y, Sunagawa K. Corticosterone-activated mineralocorticoid receptor contributes to salt-induced sympathoexcitation in pressure overload mice. *Clin Exp Hypertens* 2014; **36**: 550–556.
37 Roland BL, Krozowski ZS, Funder JW. Glucocorticoid receptor, mineralocorticoid receptors, 11 beta-hydroxysteroid dehydrogenase-1 and -2 expression in rat brain and kidney: in situ studies. *Mol Cell Endocrinol* 1995; **111**: R1–R7.
38 Roland BL, Li KX, Funder JW. Hybridization histochemical localization of 11 beta-hydroxysteroid dehydrogenase type 2 in rat brain. *Endocrinology* 1995; **136**: 4697–4700.

39 Robson AC, Leckie CM, Seckl JR, Holmes MC. 11 Beta-hydroxysteroid dehydrogenase type 2 in the postnatal and adult rat brain. *Brain Res Mol Brain Res* 1998; **61**: 1–10.

40 Geerling JC, Loewy AD. Aldosterone in the brain. *Am J Physiol Renal Physiol* 2009; **297**: F559–F576.

41 Chen J, Gomez-Sanchez CE, Penman A, May PJ, Gomez-Sanchez E. Expression of mineralocorticoid and glucocorticoid receptors in preautonomic neurons of the rat paraventricular nucleus. *Am J Physiol Regul Integr Comp Physiol* 2014; **306**: R328–R340.

42 Gomez-Sanchez CE, de Rodriguez AF, Romero DG, Estess J, Warden MP, Gomez-Sanchez MT, Gomez-Sanchez EP. Development of a panel of monoclonal antibodies against the mineralocorticoid receptor. *Endocrinology* 2006; **147**: 1343–1348.

43 Geerling JC, Kawata M, Loewy AD. Aldosterone-sensitive neurons in the rat central nervous system. *J Comp Neurol* 2006; **494**: 515–527.

44 Gomez-Sanchez EP, Ganjam V, Chen YJ, Liu Y, Zhou MY, Toroslu C, Romero DG, Hughson MD, de Rodriguez A, Gomez-Sanchez CE. Regulation of 11 beta-hydroxysteroid dehydrogenase enzymes in the rat kidney by estradiol. *Am J Physiol Endocrinol Metab* 2003; **285**: E272–E279.

45 Lombes M, Farman N, Oblin ME, Baulieu EE, Bonvalet JP, Erlanger BF, Gasc JM. Immunohistochemical localization of renal mineralocorticoid receptor by using an anti-idiotypic antibody that is an internal image of aldosterone. *Proc Natl Acad Sci USA* 1990; **87**: 1086–1088.

46 Rundle SE, Smith AI, Stockman D, Funder JW. Immunocytochemical demonstration of mineralocorticoid receptors in rat and human kidney. *J Steroid Biochem* 1989; **33**: 1235–1242.

47 Rundle SE, Funder JW, Lakshmi V, Monder C. The intrarenal localization of mineralocorticoid receptors and 11 beta-dehydrogenase: immunocytochemical studies. *Endocrinology* 1989; **125**: 1700–1704.

48 Krozowski ZS, Rundle SE, Wallace C, Castell MJ, Shen JH, Dowling J, Funder JW, Smith AI. Immunolocalization of renal mineralocorticoid receptors with an antiserum against a peptide deduced from the complementary deoxyribonucleic acid sequence. *Endocrinology* 1989; **125**: 192–198.

49 Smith RE, Li KX, Andrews RK, Krozowski Z. Immunohistochemical and molecular characterization of the rat 11 beta-hydroxysteroid dehydrogenase type II enzyme. *Endocrinology* 1997; **138**: 540–547.

50 Yamashita M, Glasgow E, Zhang BJ, Kusano K, Gainer H. Identification of cell-specific messenger ribonucleic acids in oxytocinergic and vasopressinergic magnocellular neurons in rat supraoptic nucleus by single-cell differential hybridization. *Endocrinology* 2002; **143**: 4464–4476.

51 Glasgow E, Kusano K, Chin H, Mezey E, Young WS III, Gainer H. Single cell reverse transcription-polymerase chain reaction analysis of rat supraoptic magnocellular neurons: neuropeptide phenotypes and high voltage-gated calcium channel subtypes. *Endocrinology* 1999; **140**: 5391–5401.

52 Xi D, Kusano K, Gainer H. Quantitative analysis of oxytocin and vasopressin messenger ribonucleic acids in single magnocellular neurons isolated from supraoptic nucleus of rat hypothalamus. *Endocrinology* 1999; **140**: 4677–4682.

53 Okamoto K, Yamri Y, Ooshima A, Park C, Haebara H, Matsumoto M, Tanaka T, Hazema F, Kyogoku M. Establishment of the inbred strain of the spontaneously hypertensive rats and genetic factors involved in hypertension. In: Okamoto K, ed. *Spontaneous Hypertension: Its Pathogcnesis and Complications*. Tokyo: Igaku Shoin Ltd, 1972: 1–8.

54 Teruyama R, Sakuraba M, Kurotaki H, Armstrong WE. Transient receptor potential channel m4 and m5 in magnocellular cells in rat supraoptic and paraventricular nuclei. *J Neuroendocrinol* 2011; **23**: 1204–1213.

55 Cope CL, Black E. The production rate of cortisol in man. *Br Med J* 1958; **1**: 1020–1024.

56 Draper N, Stewart PM. 11beta-hydroxysteroid dehydrogenase and the pre-receptor regulation of corticosteroid hormone action. *J Endocrinol* 2005; **186**: 251–271.

57 Gomez-Sanchez CE, Zhou MY, Cozza EN, Morita H, Foecking MF, Gomez-Sanchez EP. Aldosterone biosynthesis in the rat brain. *Endocrinology* 1997; **138**: 3369–3373.

58 Chapman K, Holmes M, Seckl J. 11beta-hydroxysteroid dehydrogenases: intracellular gate-keepers of tissue glucocorticoid action. *Physiol Rev* 2013; **93**: 1139–1206.

59 Gomez-Sanchez EP, Gomez-Sanchez MT, de Rodriguez AF, Romero DG, Warden MP, Plonczynski MW, Gomez-Sanchez CE. Immunohistochemical demonstration of the mineralocorticoid receptor, 11beta-hydroxysteroid dehydrogenase-1 and -2, and hexose-6-phosphate dehydrogenase in rat ovary. *J Histochem Cytochem* 2009; **57**: 633–641.

60 Krozowski Z, Li KX, Koyama K, Smith RE, Obeyesekere VR, Stein-Oakley A, Sasano H, Coulter C, Cole T, Sheppard KE. The type I and type II 11-beta-hydroxysteroid dehydrogenase enzymes. *J Steroid Biochem Mol Biol* 1999; **69**: 391–401.

61 Seckl JR, Yau J, Holmes M. 11Beta-hydroxysteroid dehydrogenases: a novel control of glucocorticoid action in the brain. *Endocr Res* 2002; **28**: 701–707.

62 Kotelevtsev Y, Holmes MC, Burchell A, Houston PM, Schmoll D, Jamieson P, Best R, Brown R, Edwards CR, Seckl JR, Mullins JJ. 11beta-hydroxysteroid dehydrogenase type 1 knockout mice show attenuated glucocorticoid-inducible responses and resist hyperglycemia on obesity or stress. *Proc Natl Acad Sci USA* 1997; **94**: 14924–14929.

63 Rajan V, Edwards CR, Seckl JR. 11 beta-Hydroxysteroid dehydrogenase in cultured hippocampal cells reactivates inert 11-dehydrocorticosterone, potentiating neurotoxicity. *J Neurosci* 1996; **16**: 65–70.

64 Stewart PM, Krozowski ZS. 11 beta-hydroxysteroid dehydrogenase. *Vitam Horm* 1999; **57**: 249–324.

65 Seckl JR, Walker BR. Minireview: 11beta-hydroxysteroid dehydrogenase type 1- a tissue-specific amplifier of glucocorticoid action. *Endocrinology* 2001; **142**: 1371–1376.

66 Atanasov AG, Nashev LG, Schweizer RA, Frick C, Odermatt A. Hexose-6-phosphate dehydrogenase determines the reaction direction of 11-beta-hydroxysteroid dehydrogenase type 1 as an oxoreductase. *FEBS Lett* 2004; **571**: 129–133.

67 Bujalska IJ, Draper N, Michailidou Z, Tomlinson JW, White PC, Chapman KE, Walker EA, Stewart PM. Hexose-6-phosphate dehydrogenase confers oxo-reductase activity upon 11 beta-hydroxysteroid dehydrogenase type 1. *J Mol Endocrinol* 2005; **34**: 675–684.

68 Gomez-Sanchez EP. The mammalian mineralocorticoid receptor: tying down a promiscuous receptor. *Exp Physiol* 2010; **95**: 13–18.

69 Gomez-Sanchez EP, Romero DG, de Rodriguez AF, Warden MP, Krozowski Z, Gomez-Sanchez CE. Hexose-6-phosphate dehydrogenase and 11beta-hydroxysteroid dehydrogenase-1 tissue distribution in the rat. *Endocrinology* 2008; **149**: 525–533.

70 Odermatt A, Arnold P, Stauffer A, Frey BM, Frey FJ. The N-terminal anchor sequences of 11beta-hydroxysteroid dehydrogenases determine their orientation in the endoplasmic reticulum membrane. *J Biol Chem* 1999; **274**: 28762–28770.

71 Albiston AL, Obeyesekere VR, Smith RE, Krozowski ZS. Cloning and tissue distribution of the human 11 beta-hydroxysteroid dehydrogenase type 2 enzyme. *Mol Cell Endocrinol* 1994; **105**: R11–R17.

72 Brown RW, Chapman KE, Edwards CR, Seckl JR. Human placental 11 beta-hydroxysteroid dehydrogenase: evidence for and partial purification of a distinct NAD-dependent isoform. *Endocrinology* 1993; **132**: 2614–2621.

73 Stewart PM, Murry BA, Mason JI. Human kidney 11 beta-hydroxysteroid dehydrogenase is a high affinity nicotinamide adenine

dinucleotide-dependent enzyme and differs from the cloned type I isoform. *J Clin Endocrinol Metab* 1994; **79**: 480–484.
74 Huang BS, Leenen FH. Mineralocorticoid actions in the brain and hypertension. *Curr Hypertens Rep* 2011; **13**: 214–220.
75 Gomez-Sanchez EP, Gomez-Sanchez CE. Central regulation of blood pressure by the mineralocorticoid receptor. *Mol Cell Endocrinol* 2012; **350**: 289–298.
76 Oki K, Gomez-Sanchez EP, Gomez-Sanchez CE. Role of mineralocorticoid action in the brain in salt-sensitive hypertension. *Clin Exp Pharmacol Physiol* 2012; **39**: 90–95.
77 Brody MJ, Varner KJ, Vasquez EC, Lewis SJ. Central nervous system and the pathogenesis of hypertension. Sites and mechanisms. *Hypertension* 1991; **18**(Suppl): III7–III12.
78 Rahmouni K, Sibug RM, De Kloet ER, Barthelmebs M, Grima M, Imbs JL, De Jong W. Effects of brain mineralocorticoid receptor blockade on blood pressure and renal functions in DOCA-salt hypertension. *Eur J Pharmacol* 2002; **436**: 207–216.
79 Gomez-Sanchez EP. Central hypertensive effects of aldosterone. *Front Neuroendocrinol* 1997; **18**: 440–462.
80 Gomez-Sanchez EP, Gomez-Sanchez CE. Effect of central infusion of benzamil on Dahl S rat hypertension. *Am J Physiol* 1995; **269**: H1044–H1047.
81 Gomez-Sanchez EP, Gomez-Sanchez CE. Effect of central amiloride infusion on mineralocorticoid hypertension. *Am J Physiol* 1994; **267**: E754–E758.
82 Wang H, Leenen FH. Brain sodium channels mediate increases in brain "ouabain" and blood pressure in Dahl S rats. *Hypertension* 2002; **40**: 96–100.
83 van Eekelen JA, Bohn MC, de Kloet ER. Postnatal ontogeny of mineralocorticoid and glucocorticoid receptor gene expression in regions of the rat tel- and diencephalon. *Brain Res Dev Brain Res* 1991; **61**: 33–43.
84 Teruyama R, Sakuraba M, Wilson LL, Wandrey NE, Armstrong WE. Epithelial sodium channels (ENaC) in magnocellular cells of the rat supraoptic and paraventricular nuclei. *Am J Physiol Endocrinol Metab* 2011; **302**: E273–E285.
85 Stokes JB. Disorders of the epithelial sodium channel: insights into the regulation of extracellular volume and blood pressure. *Kidney Int* 1999; **56**: 2318–2333.
86 Stockand JD. New ideas about aldosterone signaling in epithelia. *Am J Physiol Renal Physiol* 2002; **282**: F559–F576.
87 Zhang W, Xia X, Reisenauer MR, Rieg T, Lang F, Kuhl D, Vallon V, Kone BC. Aldosterone-induced Sgk1 relieves Dot1a-Af9-mediated transcriptional repression of epithelial Na^+ channel alpha. *J Clin Invest* 2007; **117**: 773–783.
88 Kempe DS, Siraskar G, Frohlich H, Umbach AT, Stubs M, Weiss F, Ackermann TF, Volkl H, Birnbaum MJ, Pearce D, Foller M, Lang F. Regulation of renal tubular glucose reabsorption by Akt2/PKBbeta. *Am J Physiol Renal Physiol* 2010; **298**: F1113–F1117.
89 Staub O, Gautschi I, Ishikawa T, Breitschopf K, Ciechanover A, Schild L, Rotin D. Regulation of stability and function of the epithelial Na^+ channel (ENaC) by ubiquitination. *EMBO J* 1997; **16**: 6325–6336.
90 Hallows KR, Bhalla V, Oyster NM, Wijngaarden MA, Lee JK, Li H, Chandran S, Xia X, Huang Z, Chalkley RJ, Burlingame AL, Pearce D. Phosphopeptide screen uncovers novel phosphorylation sites of Nedd4-2 that potentiate its inhibition of the epithelial Na^+ channel. *J Biol Chem* 2010; **285**: 21671–21678.
91 Ke Y, Butt AG, Swart M, Liu YF, McDonald FJ. COMMD1 downregulates the epithelial sodium channel through Nedd4-2. *Am J Physiol Renal Physiol* 2010; **298**: F1445–F1456.
92 Diakov A, Korbmacher C. A novel pathway of epithelial sodium channel activation involves a serum- and glucocorticoid-inducible kinase consensus motif in the C terminus of the channel's alpha-subunit. *J Biol Chem* 2004; **279**: 38134–38142.
93 Asher C, Wald H, Rossier BC, Garty H. Aldosterone-induced increase in the abundance of Na+ channel subunits. *Am J Physiol* 1996; **271**: C605–C611.
94 Pacha J, Frindt G, Antonian L, Silver RB, Palmer LG. Regulation of Na channels of the rat cortical collecting tubule by aldosterone. *J Gen Physiol* 1993; **102**: 25–42.
95 Frindt G, Sackin H, Palmer LG. Whole-cell currents in rat cortical collecting tubule: low-Na diet increases amiloride-sensitive conductance. *Am J Physiol* 1990; **258**: F562–F567.
96 Huang BS, White RA, Jeng AY, Leenen FH. Role of central nervous system aldosterone synthase and mineralocorticoid receptors in salt-induced hypertension in Dahl salt-sensitive rats. *Am J Physiol Regul Integr Comp Physiol* 2009; **296**: R994–R1000.
97 Kawamura A, Guo J, Itagaki Y, Bell C, Wang Y, Haupert GT Jr, Magil S, Gallagher RT, Berova N, Nakanishi K. On the structure of endogenous ouabain. *Proc Natl Acad Sci USA* 1999; **96**: 6654–6659.
98 Huang BS, White RA, Ahmad M, Jeng AY, Leenen FH. Central infusion of aldosterone synthase inhibitor prevents sympathetic hyperactivity and hypertension by central Na+ in Wistar rats. *Am J Physiol Regul Integr Comp Physiol* 2008; **295**: R166–R172.
99 MacKenzie SM, Clark CJ, Fraser R, Gomez-Sanchez CE, Connell JM, Davies E. Expression of 11beta-hydroxylase and aldosterone synthase genes in the rat brain. *J Mol Endocrinol* 2000; **24**: 321–328.
100 Stricker EM, Wolf G. Blood volume and tonicity in relation to sodium appetite. *J Comp Physiol Psychol* 1966; **62**: 275–279.
101 Stricker EM. Effects of hypovolemia and-or caval ligation on water and NaCl solution drinking by rats. *Physiol Behav* 1971; **6**: 299–305.
102 Epstein AN. Mineralocorticoids and cerebral angiotensin may act together to produce sodium appetite. *Peptides* 1982; **3**: 493–494.
103 Toth E, Stelfox J, Kaufman S. Cardiac control of salt appetite. *Am J Physiol* 1987; **252**: R925–R929.
104 Formenti S, Bassi M, Nakamura NB, Schoorlemmer GH, Menani JV, Colombari E. Hindbrain mineralocorticoid mechanisms on sodium appetite. *Am J Physiol Regul Integr Comp Physiol* 2013; **304**: R252–R259.
105 Blackburn RE, Samson WK, Fulton RJ, Stricker EM, Verbalis JG. Central oxytocin and ANP receptors mediate osmotic inhibition of salt appetite in rats. *Am J Physiol* 1995; **269**: R245–R251.
106 Arletti R, Benelli A, Bertolini A. Oxytocin inhibits food and fluid intake in rats. *Physiol Behav* 1990; **48**: 825–830.
107 Blackburn RE, Demko AD, Hoffman GE, Stricker EM, Verbalis JG. Central oxytocin inhibition of angiotensin-induced salt appetite in rats. *Am J Physiol* 1992; **263**: R1347–R1353.
108 Fitts DA, Thornton SN, Ruhf AA, Zierath DK, Johnson AK, Thunhorst RL. Effects of central oxytocin receptor blockade on water and saline intake, mean arterial pressure, and c-Fos expression in rats. *Am J Physiol Regul Integr Comp Physiol* 2003; **285**: R1331–R1339.
109 Rigatto K, Puryear R, Bernatova I, Morris M. Salt appetite and the renin-angiotensin system: effect of oxytocin deficiency. *Hypertension* 2003; **42**: 793–797.
110 Krause EG, Sakai RR. Richter and sodium appetite: from adrenalectomy to molecular biology. *Appetite* 2007; **49**: 353–367.
111 Stricker EM, Verbalis JG. Central inhibition of salt appetite by oxytocin in rats. *Regul Pept* 1996; **66**: 83–85.
112 Roesch DM, Blackburn-Munro RE, Verbalis JG. Mineralocorticoid treatment attenuates activation of oxytocinergic and vasopressinergic neurons by icv ANG II. *Am J Physiol Regul Integr Comp Physiol* 2001; **280**: R1853–R1864.
113 Grafe LA, Takacs AE, Yee DK, Flanagan-Cato LM. The role of the hypothalamic paraventricular nucleus and the organum vasculosum

lateral terminalis in the control of sodium appetite in male rats. *J Neurosci* 2014; **34**: 9249–9260.
114 Chiaraviglio E, Perez Guaita MF. The effect of intracerebroventricular hypertonic infusion on sodium appetite in rats after peritoneal dialysis. *Physiol Behav* 1986; **37**: 695–699.
115 Watanabe E, Fujikawa A, Matsunaga H, Yasoshima Y, Sako N, Yamamoto T, Saegusa C, Noda M. Nav2/NaG channel is involved in control of salt-intake behavior in the CNS. *J Neurosci* 2000; **20**: 7743–7751.
116 Weisinger RS, Denton DA, McKinley MJ. Self-administered intravenous infusion of hypertonic solutions and sodium appetite of sheep. *Behav Neurosci* 1983; **97**: 433–444.
117 Doi Y, Nose H, Morimoto T. Changes in Na concentration in cerebrospinal fluid during acute hypernatremia and their effect on drinking in juvenile rats. *Physiol Behav* 1992; **52**: 499–504.
118 Weisinger RS, Considine P, Denton DA, McKinley MJ. Rapid effect of change in cerebrospinal fluid sodium concentration on salt appetite. *Nature* 1979; **280**: 490–491.
119 Weisinger RS, Considine P, Denton DA, Leksell L, McKinley MJ, Mouw DR, Muller AF, Tarjan E. Role of sodium concentration of the cerebrospinal fluid in the salt appetite of sheep. *Am J Physiol* 1982; **242**: R51–R63.

